Molecular Therapy
Oncolytics
Original Article

Fidarestat induces glycolysis of NK cells through decreasing AKR1B10 expression to inhibit hepatocellular carcinoma

Tiangen Wu,[1,2,3] Yang Ke,[1,3] Haoran Tang,[2,3] Chen Liao,[2,3] Jinze Li,[1,3] and Lin Wang[1]

[1]Department of Hepatobiliary Surgery, The Second Affiliated Hospital of Kunming Medical University, No. 374, Dianmian Avenue, Kunming 650101, China; [2]Department of Gastroenterological Surgery, The Second Affiliated Hospital of Kunming Medical University, Kunming 650101, China

The aldose reductase inhibitor Fidarestat has been noted to have efficacy in treating a variety of tumors. To define its role in hepatocellular carcinoma (HCC), we induced a HCC xenograft model in mice, which were treated with different doses of Fidarestat. The amounts of natural killer (NK) cells and related inflammatory factors were detected in the serum of the mice. Fidarestat inhibited HCC tumor growth and lung metastasis *in vivo* and increased NK cell number as well as levels of NK cell-related inflammatory factors in mouse serum. NK cells were then co-cultured with the HCC cell line *in vitro* to detect effects on HCC cell progression after Fidarestat administration. The glycolysis activity of the NK cells was evaluated by extracellular acidification rate, while aldo-keto reductase family 1 member B10 (AKR1B10) expression was detected by western blot analysis. Administration of Fidarestat downregulated the expression of AKR1B10 in NK cells and promoted NK cell glycolysis to enhance their killing activity against HCC cells. However, depletion of NK cells or upregulation of AKR1B10 attenuated the anticancer activity of Fidarestat. Taken together, Fidarestat downregulated AKR1B10 expression in NK cells to promote NK cell glycolysis, thereby alleviating HCC progression.

INTRODUCTION

Hepatocellular carcinoma (HCC) is the most common form of liver cancer.[1] According to the Surveillance, Epidemiology, and End Results (SEER) study, the incidence of HCC will continue to rise over the next 10–20 years and peak around 2030.[2] Although improvements in diagnostic methods and surgical techniques have led to improved clinical management of HCC, the annual mortality rate associated with HCC has increased significantly over the past 20 years.[3] The most significant factors contributing to this state of affairs are the lack of biomarkers to identify tumors in relation to stage of progression or metastasis, drug resistance, and the extent of intra-tumor heterogeneity.[4] In addition, the unclear molecular mechanisms of hepatocyte malignant transformation further complicate the discovery of more effective HCC treatments.[5] Therefore, there is an urgent need to identify reliable prognostic biomarkers and to discover specific therapeutic targets for HCC.[6]

Immune cells are key players in the host's defense against infection and cancer. In response to threat signals, the metabolism of immune cells constantly changes to adjust immune function.[7] Modulation of different metabolic states of different immune cells in the tumor microenvironment may provide a means to artificially interfere with immune cell function.[8] It is well known that tumor-infiltrating immune cells are abundantly present in the tumor microenvironment, among which are the natural killer (NK) cells, which normally account for 25%–50% of the total number of lymphocytes in the healthy liver,[9] suggesting that NK cells may exert important effects on the immune function of the liver. However, in patients with advanced HCC, NK cells usually show reduced infiltration and impaired function, such as reduced production of tumor necrosis factor alpha (TNF-α) and interferon gamma (IFN-γ).[10] Recently, immune cell metabolism has received research attention. Because of nutrient and oxygen deficiencies and locally high concentrations of tumor-derived metabolic wastes such as lactic acid, NK cells in the tumor microenvironment show impaired metabolism and effector functions.[11]

Aldo-keto reductase family 1 member B8 (AKR1B8), and its human orthologue AKR1B10, are NADPH-dependent enzymes that can reduce a variety of carbonyl substrates [12]. Recently, AKR1B10 has been consistently reported to be overexpressed in various solid cancers such as cholangiocarcinoma,[13]pancreatic cancer,[14]breast cancer,[15]and HCC.[16]AKR1B10 thus has been recognized as a valuable biomarker and prognostic indicator for several cancers.[17,18] Higher AKR1B10 expression in tumors is significantly associated with dismal overall survival in HCC patients.[19]Wang et al.[20]have verified the oncogenic function of AKR1B10 in the HCC cell lines SMMC-7721, HepG2, and Hep3B. Interestingly, AKR1B10 is a transcriptional target of p53, which is involved in a wide range of cellular metabolic pathways, including glycolysis.[21]Based on these, we hypothesize that AKR1B10 may regulate glycolysis and lactate metabolism in NK cells. Importantly, the aldose reductase inhibitor Fidarestat can directly

Received 15 December 2020; accepted 8 June 2021;
https://doi.org/10.1016/j.omto.2021.06.005.

[3]These authors contributed equally

Correspondence: Lin Wang, Department of Hepatobiliary Surgery, The Second Affiliated Hospital of Kunming Medical University, No. 374, Dianmian Avenue, Kunming 650101, Yunnan Province, P.R. China.
E-mail: linwang0705@126.com

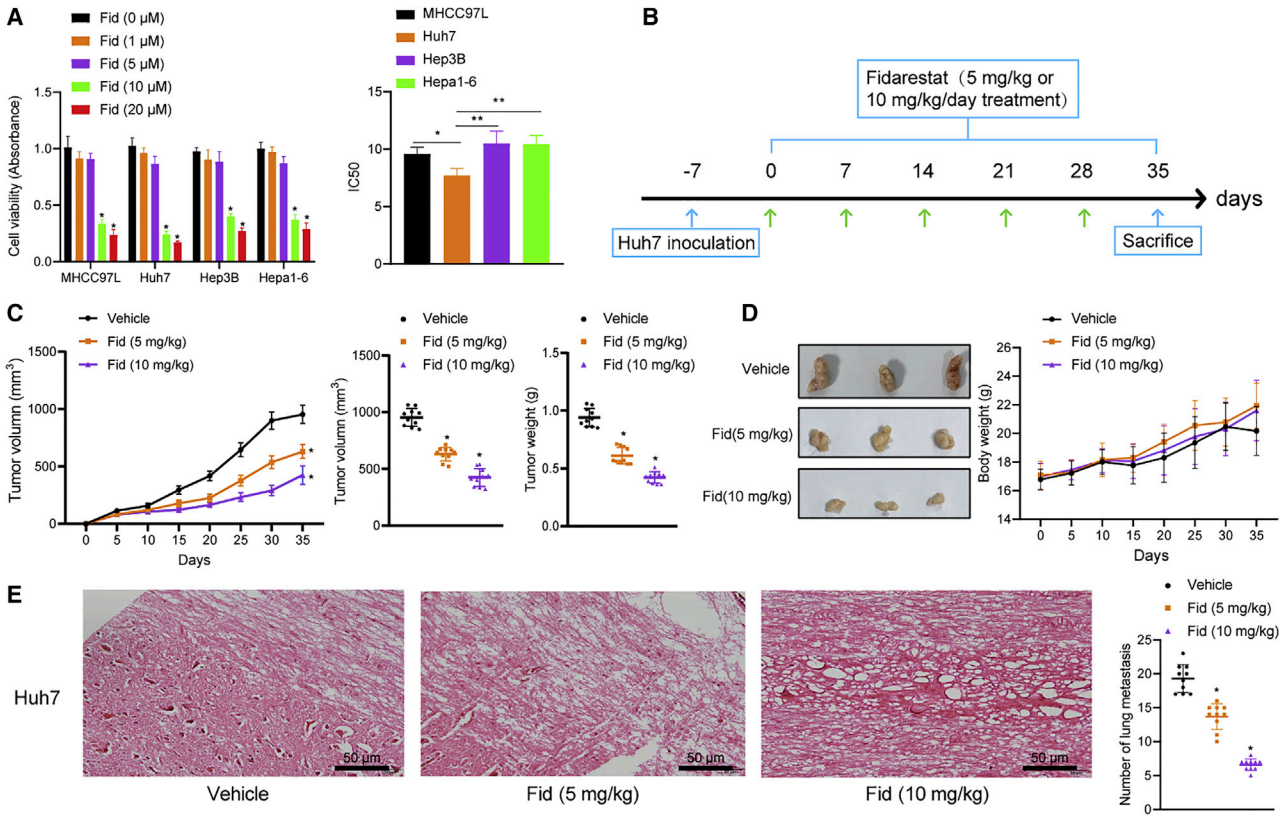

Figure 1. Inhibitory effect of Fidarestat on nude mouse HCC xenograft tumors

(A) Cell viability of MHCC97L, Huh7, Hep3B, and Hepa1-6 cell lines upon treatment with different concentrations of Fidarestat (0, 1, 5, 10, and 20 μM). (B) Schematic diagram of experimental procedure of Huh7 cell inoculation in nude mice. (C) Tumor volume of tumor-bearing nude mice upon administration of Fidarestat (5 or 10 mg/kg) or vehicle. (D) The effect of Fidarestat on tumor weight of Huh7 xenograft, 35 weeks after administration. (E) Lung metastasis upon treatment with Fidarestat or vehicle (magnification, ×200). *$p < 0.05$ versus vehicle. n = 10, cell experiments were repeated in triplicate, and multiple comparison was analyzed by one-way ANOVA or repeated-measures ANOVA.

inhibit AKR1B10 expression,[22] and Fidarestat has been shown to have efficacy in treating a variety of tumors.[23] However, little is known about the effect of Fidarestat on HCC and its regulatory mechanism.

To investigate the anti-tumor effect of Fidarestat in HCC, we constructed a nude mouse model xenografted with HCC tumor and co-cultured NK cells with the HCC cell line *in vitro* to detect effects of Fidarestat administration on HCC cell progression.

RESULTS

Fidarestat inhibits tumor growth and lung metastasis in tumor-bearing nude mice

In order to study the effect of Fidarestat on HCC cells in tumor-bearing nude mice, we administered different concentrations of Fidarestat to HCC cell lines MHCC97L, Huh7, Hep3B, and Hepa1-6 to screen an optimum inhibitory concentration and the most sensitive cell line. As shown in Figure 1A, Fidarestat at concentrations of 1 and 5 μM rarely exerted inhibitory activity on each cell line, while Fidarestat at 10 and 20 μM had an inhibitory effect on cells, with the Huh7 cell line showing the most significant reduction in cell viability. Therefore, we chose Huh7 cells for the following experiments in which the concentration of Fidarestat was set at 10 μM. Next, nude mice were subcutaneously injected with Huh7 cells as well as Fidarestat or saline. We found that the tumor volume of mice increased with time; however, administration of Fidarestat had a significant inhibitory effect on tumor growth *in vivo* (Figures 1B and 1C). In contrast, compared with saline treatment, administration of Fidarestat did not significantly decrease the body weight of tumor-bearing nude mice, and there was no attrition during treatment, indicating that Fidarestat at 5 or 10 mg/kg/day exhibits weak toxicity (Figure 1D). Mice were euthanized 35 days after the Huh7 cell administration, and the tumors were weighed, showing that Fidarestat significantly reduced tumor weight compared with saline treatment. Furthermore, we took lung samples from the Huh7-cells-inoculated mice and performed hematoxylin and eosin (H&E) staining, which revealed that Fidarestat inhibited metastatic lung tumor formation in the tumor-bearing nude mice, accompanied by markedly reduced lung metastatic nodules, to an extent dependent on the Fidarestat dose (Figure 1E). These

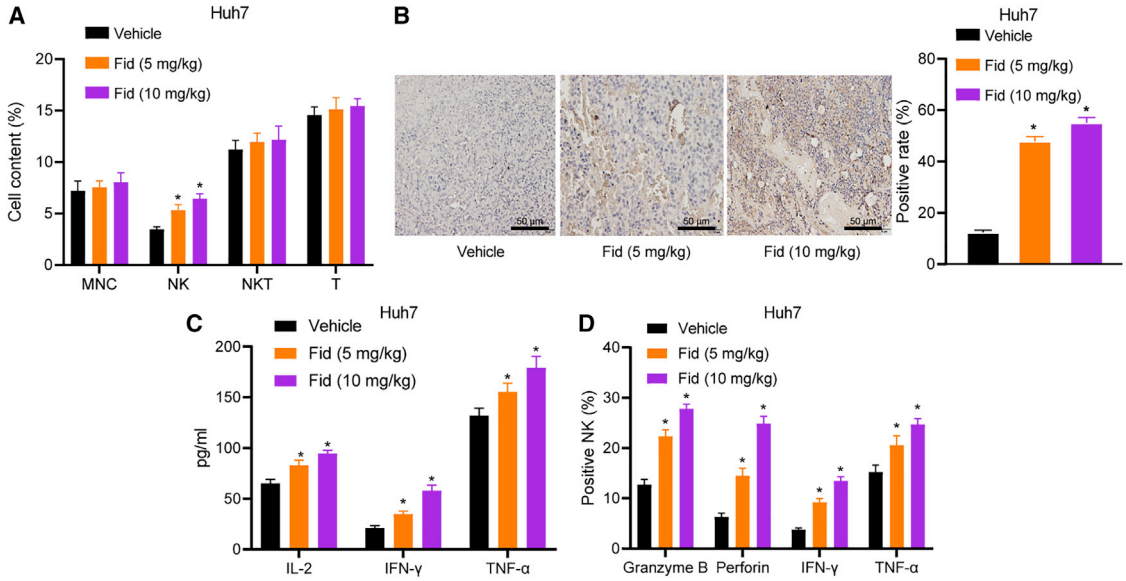

Figure 2. The anticancerous effect of Fidarestat on the number and function of immune cells

(A) Quantification of the number of MNCs, NK cells, NKT cells, and T cells in Huh7-cells-induced mouse model upon treatment with Fidarestat or vehicle. (B) NK cells in Huh7-cells-inoculated mice xenografted with tumor were detected by IHC upon treatment with Fidarestat or vehicle. (C) The levels of NK cell-related inflammatory factors (IL-2, IFN-γ, and TNF-α) in serum of Huh7 cell tumor-bearing mice detected by ELISA. (D) The proportion of NK cells positive for granzyme B, perforin, IFN-γ, or TNF-α analyzed by flow cytometry in Huh7 cells of tumor-bearing mice upon treatment with Fidarestat or vehicle. *p < 0.05 versus vehicle. n = 10, multiple comparison was analyzed by one-way ANOVA.

results elucidated that Fidarestat exerted a prominently inhibitory effect on tumor growth and metastasis in HCC.

Fidarestat regulates tumor microenvironment and exerts anti-HCC effect

Fidarestat has been reported to suppress the malignant phenotype of tumors.[24] We speculated that Fidarestat could adjust the function of immune cells to exert anticancer effects. Therefore, we measured immune factors and the abundances of several common immune cells including mononuclear cells (MNCs), NK cells, T cells, and NK T (NKT) cells to analyze the composition of immune cells after Fidarestat treatment. We found that in the Huh7-cells-induced HCC model mice, Fidarestat administration did not significantly change the number of MNCs, T cells, and NKT cells, but remarkably increased the number of NK cells, indicating that Fidarestat may affect NK cells to exert anti-tumor activity (Figure 2A). In addition, we stained NK cells with NK1.1 and found that the proportion of NK cells was significantly elevated in Fidarestat-treated tumor tissues, suggesting that Fidarestat can recruit NK cells to tumor tissues (Figure 2B). Previous evidence has demonstrated that interleukin-2 (IL-2), IFN-γ, and TNF-α are key factors in the anticancer activity of NK cells.[25] Therefore, we measured the levels of IL-2, IFN-γ, and TNF-α in serum using enzyme-linked immunosorbent assay (ELISA), which displayed that the presence of Fidarestat significantly upregulated the levels of these cytokines, implying that Fidarestat may exert its anti-tumor activity by enhancing cytokine secretion of NK cells (Figure 2C). Next, we isolated primary NK cells to detect NK cell-killing and activation-related molecules. As reflected by flow cytometry, Fidarestat treatment upregulated the proportion of NK cells positive for granzyme B, perforin, IFN-γ, and TNF-α, indicating that Fidarestat may exert its anti-tumor activity by increasing the degranulation and cytokine secretion of NK cells (Figure 2D; Figure S1). Collectively, we find that Fidarestat alleviated HCC through activating the anti-tumor activity of NK cells and mediating microenvironment.

Fidarestat promotes NK cell function to inhibit HCC cell proliferation, invasion, and metastasis *in vitro*

To explore the role of Fidarestat in the killing ability of NK cells, NK cells were co-cultured with Huh7 cells or normal liver cells HL-7702 at different multiplicities of infection (MOIs). We found that Fidarestat at a concentration of 10 μM increased the killing activity of NK cells against HCC cells. Furthermore, as the proportion of NK cells in MOI increased, the cytotoxicity of NK cells was further enhanced by Fidarestat, indicating that Fidarestat can indeed enhance NK cell-killing activity in HCC cells (Figure 3A). However, Fidarestat did not increase the killing activity of NK cells in HL-7702 cells (Figure 3B). The results of Transwell assays showed that Fidarestat promoted the inhibitory effects of NK cells on the invasion of Huh7 cells (Figure 3C). Moreover, NK cells treated with Fidarestat further inhibited the migration of Huh7 cells (target cells/NK cells = 1:10) (Figure 3D). Therefore, Fidarestat inhibited the invasion and migration of HCC cells via NK cells *in vitro*.

Fidarestat promotes NK cell function to inhibit HCC *in vivo*

We then proceeded to explore whether Fidarestat increased the anti-tumor activity of NK cells. First, we performed *in vitro* experiments using

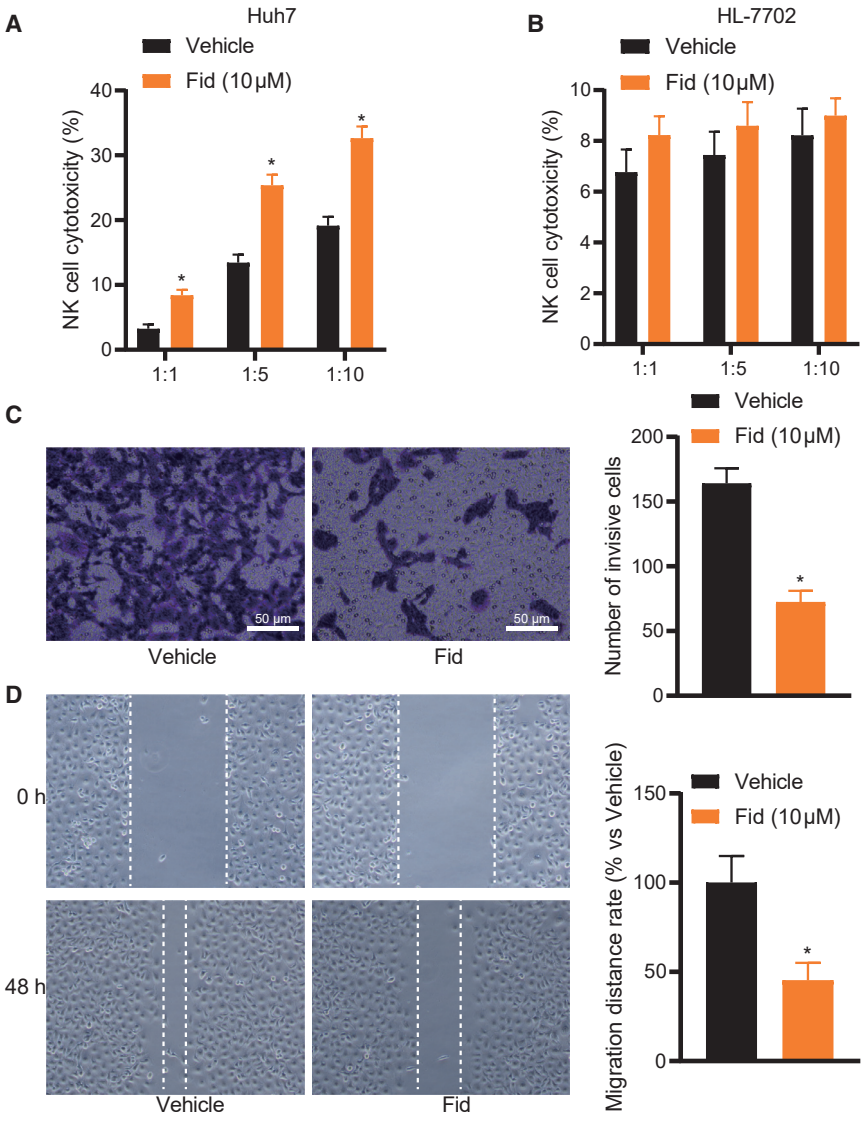

Figure 3. Fidarestat promotes NK cell killing

(A) Quantification of NK cell cytotoxicity upon treatment with Fidarestat-treated Huh7 cells. (B) Quantification of NK cell cytotoxicity when NK cells were co-cultured with normal liver cell lines upon treatment with Fidarestat or vehicle. (C) Transwell assay (magnification, ×200) of cell invasion of Huh7 cells co-cultured with NK cells in the presence or absence of Fidarestat or vehicle and corresponding quantification. (D) Transwell assay of cell migration of Huh7 cells upon co-culture with NK cells and treatment with Fidarestat or vehicle. *$p < 0.05$ versus vehicle. Experiments were repeated for 3 times, and comparison between two groups was analyzed by unpaired t test, and in (A) and (B), one-way ANOVA was applied.

10 μM Fidarestat or 10 μM Fidarestat combined with 1:10 target ratio of NK cells co-cultured with Huh7 cells. The results showed that, compared with the saline treatment, 10 μM Fidarestat treatment had a significant inhibitory effect on Huh7 cells and that the inhibitory effect was significantly enhanced following treatment of Fidarestat combined with NK cells compared with Fidarestat treatment only (Figure 4A). Next, we established a xenografted nude model followed by depletion of NK cells. As shown in Figure 4B, Fidarestat administration was followed by an increased infiltration of NK cells in the tumor sections, while NK cell-depleting agent anti-NK1.1 significantly inhibited the recruitment of NK cells to tumor tissues *in vivo* (Figure 4C). Consistent with previous results, administration of Fidarestat inhibited tumor growth, which manifested as a decrease in tumor volume and weight (Figures 4D and 4E). In addition, Fidarestat inhibited the metastasis of tumor cells to the lungs, along with fewer lung metastatic nodules, but the addition of anti-NK1.1 significantly weakened the efficacy of Fidarestat, as demonstrated by increased tumor growth and metastasis as well as increased numbers of lung metastatic nodules (Figure 4F). Therefore, Fidarestat inhibited HCC progression by enhancing the function of NK cells *in vivo* and *in vitro*.

Fidarestat downregulates the expression of AKR1B10 and promotes glycolysis

Fidarestat has attracted much attention due to its ability to regulate blood sugar in the context of diabetes and diabetic neuropathy; NK cells can exert their anti-tumor activity by affecting glucose metabolism.[26] In addition, AKR1B10 could reduce the glycolytic capacity of tumor cells.[27] To study whether Fidarestat regulated the expression of AKR1B10 to promote glycolysis in NK cells, we treated Huh7 tumor-bearing nude mice with Fidarestat for 35 days and then isolated primary NK cells to test their glycolytic ability (Figure 5A). The results of extracellular acidification rate (ECAR) assays showed that the addition of glucose decreased the glycolytic capacity of NK cells, whereas Fidarestat treatment facilitated the glycolytic capacity of NK cells. Furthermore, addition of Oligomycin A inhibited oxidative phosphorylation and increased lactic acid production, while 2-deoxy-glucose (2-DG) treatment hardly influenced glycolytic ability (Figure 5B). In addition, through analyzing the area under the ECAR curve, we found that Fidarestat at doses of 5 or 10 mg/kg significantly enhanced the glycolytic capacity of primary NK cells (Figure 5C). Moreover, as reflected by western blot, Fidarestat downregulated the expression of AKR1B10 in NK cells (Figure 5D). Next, we explored the effect of Fidarestat on the glycolytic capacity of NK cells. The results showed that Fidarestat promoted glycolytic capacity and lactic acid production of NK cells (Figures 5E and 5F). By analyzing the expression of AKR1B10 protein in NK cells, we showed that Fidarestat can downregulate AKR1B10, which was consistent with the results with primary NK cells (Figure 5G). The above-mentioned results indicated that Fidarestat could reduce AKR1B10 expression and promote glycolysis.

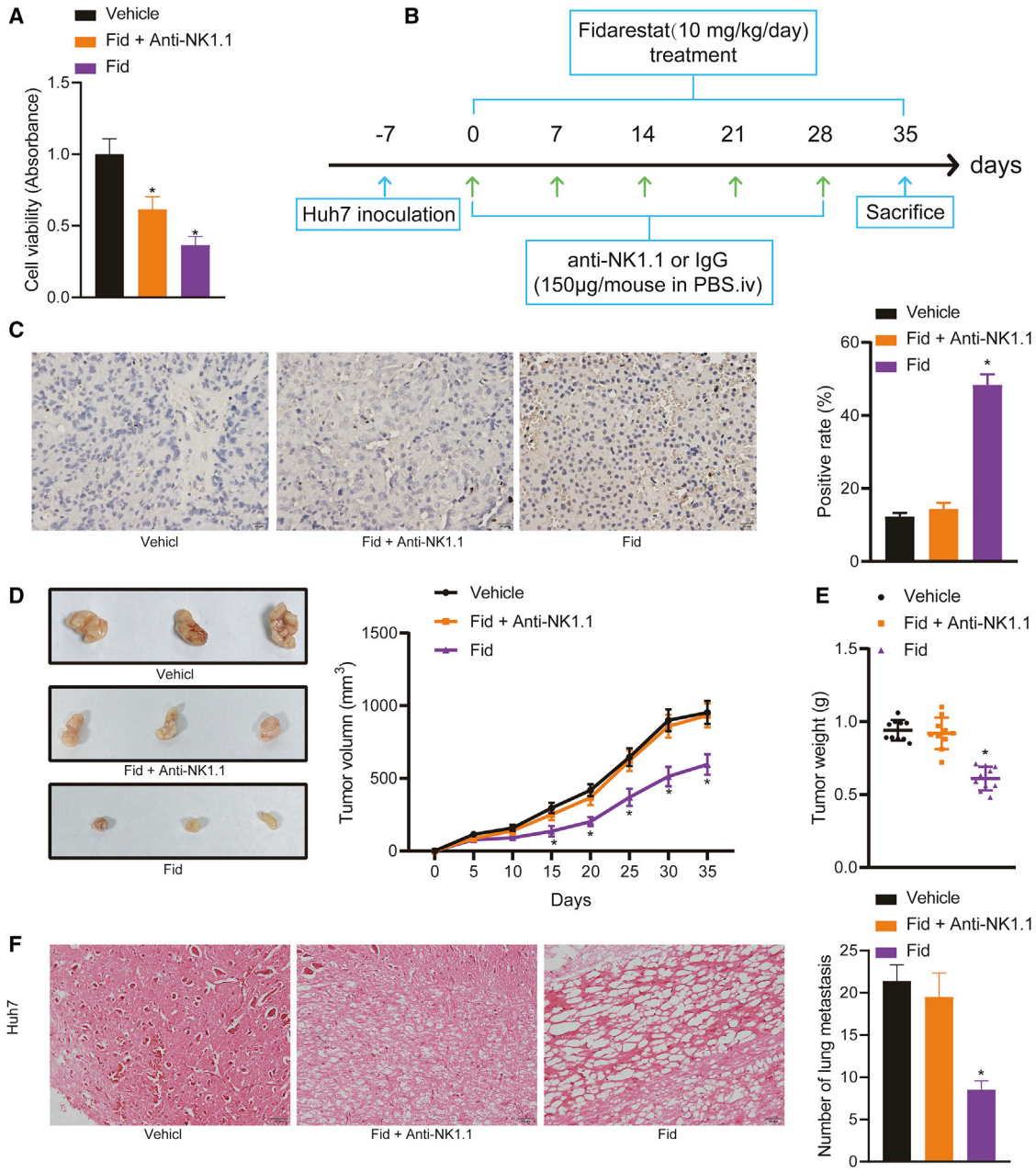

Figure 4. Depletion of NK cells reduces the effect of Fidarestat on HCC *in vivo*

(A) Inhibitory effect of Fidarestat or Fidarestat combined with NK cells co-cultured with Huh7 cells. (B) Schematic diagram of NK cell depletion experiment procedure. (C) NK cell infiltration in tumor tissues upon treatment with Fidarestat or anti-NK1.1. (D) Tumor volume in Huh7 cell tumor-bearing nude mice treated with Fidarestat or anti-NK1.1. (E) Tumor weight in Huh7 cell tumor-bearing nude mice treated with Fidarestat or anti-NK1.1. (F) Representative H&E images of lung metastasis in Huh7 cell tumor-bearing nude mice treated with Fidarestat or anti-NK1.1 (magnification, ×200). *$p < 0.05$ versus vehicle. n = 10, multiple comparison was analyzed by one-way ANOVA or repeated-measures ANOVA.

Fidarestat exerts its anticancer activity by inhibiting AKR1B10 expression and promoting glycolysis of NK cells

In an attempt to understand whether Fidarestat regulated the expression of AKR1B10 to promote anticancer activity in NK cells, we constructed an AKR1B10 overexpression plasmid and validated its efficiency. In addition, the results from western blot analysis also showed that Fidarestat treatment alone inhibited AKR1B10 expression and that overexpression of AKR1B10 restored its expression (Figure 6A). Administration of Fidarestat enhanced NK cell glycolysis and the production of lactic acid. Empty vector treatment exerted no

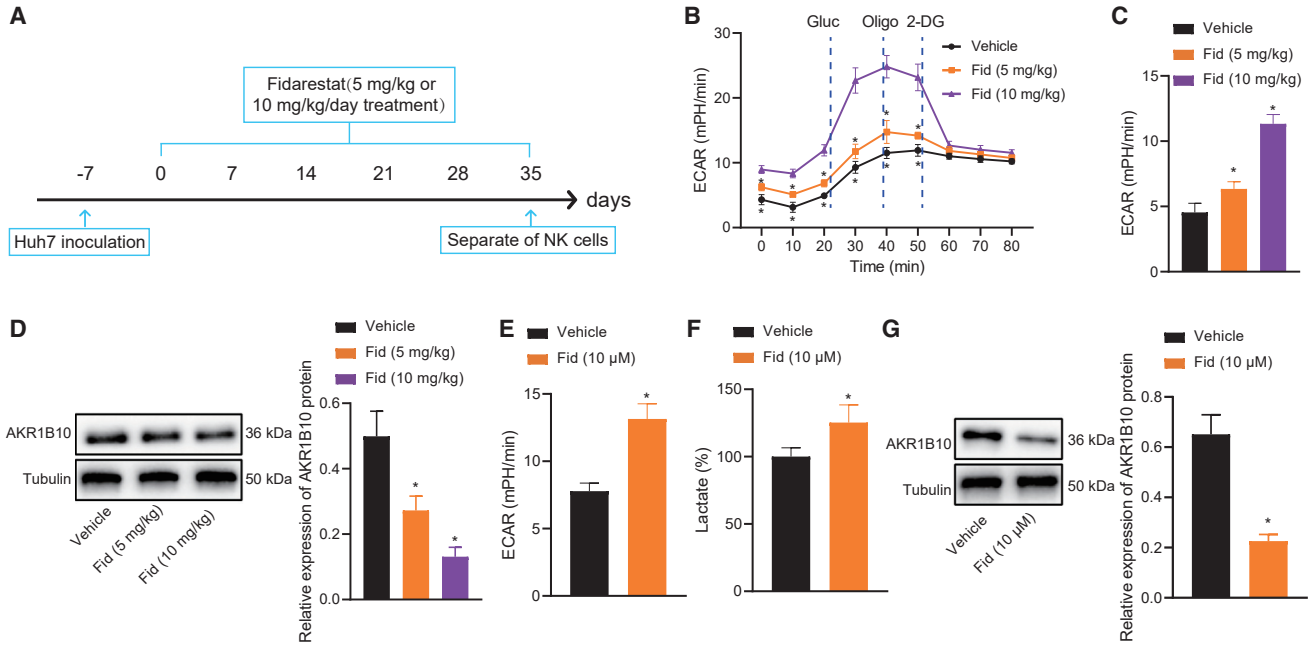

Figure 5. Fidarestat promotes glycolysis and inhibits AKR1B10 in primary NK cells

(A) The experimental process of primary NK cell extraction. (B) Glycolysis rate detected in Huh7 tumor-bearing nude mice by ECAR. (C) The area under the curve of ECAR. (D) AKR1B10 in primary NK cells detected with or without Fidarestat treatment by western blot. (E) NK cell glycolysis assay. (F) Lactic acid produced by NK cells. (G) AKR1B10 protein expression in NK cells detected by western blot. *$p < 0.05$. Experiments were repeated three times, and comparison between two groups was analyzed by un-paired t test and among multiple groups was analyzed by one-way ANOVA or two-way ANOVA for data under different concentrations.

significant effect on cell glycolysis and the production of lactic acid, but further overexpressing AKR1B10 in HCC cells weakened the effect of Fidarestat on glycolysis and lactic acid production, indicating that Fidarestat promotes NK cell glycolysis via inhibition of AKR1B10 (Figures 6B and 6C). Additionally, under conditions of overexpressed AKR1B10, NK cells were co-cultured with Huh7 cells; we then observed that NK cells overexpressing AKR1B10 exerted decreased killing activity on Huh7 cells after Fidarestat treatment (Figure 6D). Moreover, the Transwell assay demonstrated inhibited migration and invasion capacities of Huh7 cells upon co-culture with NK cells with overexpressed AKR1B10, followed by Fidarestat administration (Figures 6E and 6F). These results demonstrated that AKR1B10 was a mediator for Fidarestat to exert its anti-tumor effect.

DISCUSSION

Despite advances in the understanding of risk factors for hepatocarcinogenesis, as well as in the diagnosis and clinical management of the disease, the molecular mechanisms of hepatocarcinogenesis are still poorly understood.[28]The liver is a key frontline immune tissue, which is equipped to detect, capture, and clear bacteria, viruses, and macromolecules.[29]Indeed, the liver is able to mount a rapid and robust immune response. Previous knowledge on the possible role of AKR1B10 in HCC has been limited to hepatocytes in the contexts of lipogenesis, oxidative stress, and detoxification of cytotoxic carbonyl compounds.[30]But how AKR1B10 may affect HCC progression by modulating the function of immune cells has been unknown. In this study, by constructing the HCC xenograft model in nude mice, we found that inhibition of AKR1B10 expression in NK cells promoted glycolysis of NK cells and suppressed migration, invasion, and lung metastasis of HCC cells *in vivo*. Inhibition of AKR1B10 expression was achieved by administration of Fidarestat, which promoted the number of infiltrating NK cells and their cytokine secretion (Figure 7).

The aldose reductase inhibitor Fidarestat has shown anti-tumor effects in a variety of cancers; for example, aldose reductase promotes colon cancer cell invasion and migration and Fidarestat inhibits these events.[23] However, the role of Fidarestat in HCC is not known. Under normal conditions, human liver aldose reductase levels are extremely low, but aldose reductase is overexpressed in the liver under conditions of oxidative stress and inflammation-related pathological conditions, such as alcoholic cirrhosis, heart failure, vascular inflammation, and cancer.[31]These findings suggest that Findarastat may have an anti-HCC effect. In the study, we inoculated nude mice with HCC cells in the presence or absence of Fidarestat treatment; mice receiving Fidarestat showed lower HCC tumor volume and lung metastasis, with little sign of toxicity, as indicated by body weight and overall survival of the mice. This was consistent with a previous report on airway epithelial cells that Fidarestat could be used as a therapeutic agent due to its low side effects *in vivo*.[32]

In the liver, the percentage of NK cells in total lymphocytes is about five times than that in the peripheral blood or spleen. As such, NK

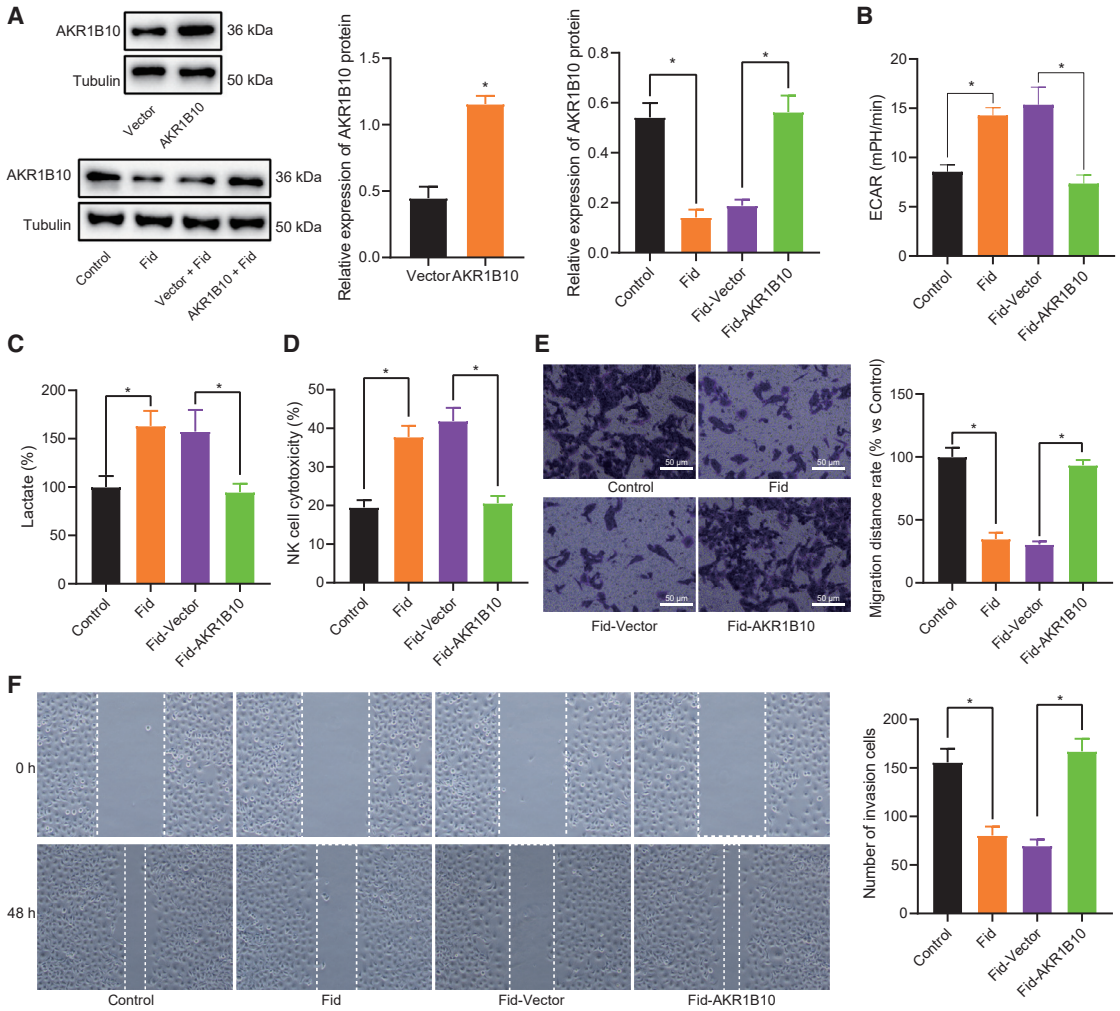

Figure 6. Overexpression of AKR1B10 in NK cells attenuates the anticancer activity of Fidarestat

(A) Western blot analysis of AKR1B10 in NK cells upon treatment with the blank vector, overexpressed AKR1B10, or Fidarestat. (B) NK cell glycolysis assessed after overexpression of AKR1B10. (C) Lactic acid metabolism in NK cells detected after overexpression of AKR1B10. (D) NK cell killing to Huh7 cells detected after treatment with vector overexpressed AKR1B10 in the presence or absence of Fidarestat. (E) The effect of AKR1B10 overexpression on the migration of Huh7 cells determined by scratch test. (F) The effect of AKR1B10 overexpression on the invasion of Huh7 cells detected by Transwell assay upon treatment with vector, overexpressed AKR1B10, or Fidarestat. *$p < 0.05$. Experiments were repeated in triplicate, and comparison between two groups was analyzed by un-paired t test and among multiple groups was analyzed by one-way ANOVA.

cells are considered to play a very important role in the prevention of HCC and serve as a potential resource for cell therapy in the treatment of HCC.[33] However, the efficacy of NK cells in the treatment of solid tumors has been unsatisfactory.[34] One of the main reasons for this limitation is the immunosuppressive effect of the tumor microenvironment. NK cells in liver tumor tissue are less numerous and show impaired cytotoxicity as well as lower IFN-γ production.[10,35] $CD8^+$ T cell cytotoxicity is dependent on granule exocytosis and more specifically, the release of granzyme B.[36] The granzyme B delivery system might contribute to cancer treatment in analogy to cytotoxic T lymphocyte (CTL)/NK cell-induced immunotherapy,[37] since NK cells play a central role in pathogenesis by utilizing granzyme B to kill virally infected target cells.[38] The mRNA levels of CD8, perforin, and granzyme B are markedly increased in HCC tumors when the disease condition is inhibited.[39] Consistently, in the present study, we found that granzyme B and perforin expression was increased in HCC cells and tissues upon administration of Fidarestat or treatment through downregulation of AKR1B10. In addition, we found that Fidarestat treatment increased the number of tumor-infiltrating NK cells, as well as serum levels of NK cell-associated inflammatory factors in the mouse HCC model, whereas administration of Fidarestat enhanced the inhibitory effect of NK cells on migration and invasion of HCC cells.

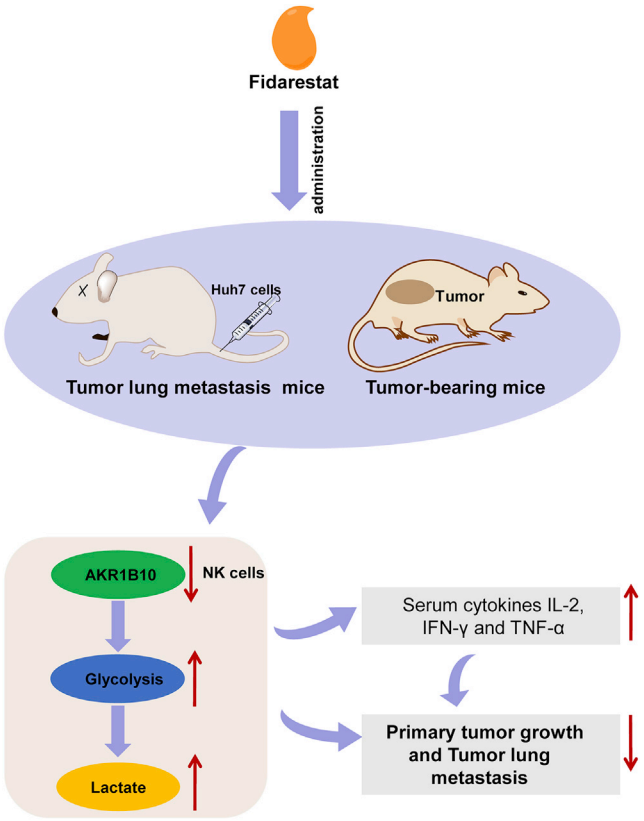

Figure 7. Schematic map of functional role of Fidarestat in HCC

Fidarestat downregulated AKR1B10 in NK cells to promote NK cell glycolysis, thereby alleviating HCC progression.

AKR1B10 is aberrantly overexpressed in many malignant tumors,[40] where it may promote tumor progression by blocking intracellular toxic carbonyl-mediated apoptosis.[41] As a promising anti-tumor agent, AKR1B10 has been targeted for the development of effective and specific inhibitors, [42,43] of which Fidarestat is a notable example. We found by western blot analysis that Fidarestat downregulated AKR1B10 expression in NK cells. In tumor tissues, high oxygen consumption of tumor cells and disordered angiogenesis can produce hypoxic regions,[44] where NK cell effector function is impaired and glycolytic metabolism is suppressed.[45,46] In this study, by transfecting NK cells with AKR1B10 overexpression plasmids, we found that overexpression of AKR1B10 inhibited NK cell glycolysis, which could be disrupted by Fidarestat. This result was also validated in the xenograft model. Notably, the progression of metastatic cancer depends on an adequate blood supply to tumor cells.[47] One study showed that aldose reductase inhibition *in vitro* suppresses vascular endothelial growth factor and the formation of capillary-like structures.[48] Whether this mechanism underlies the inhibition of HCC lung metastasis by Fidarestat shown in this study warrants further investigation.

In the present study, we have demonstrated part of the mechanism by which Fidarestat inhibited the proliferation, migration, and invasion of HCC cells. The *in vitro* results showed that Fidarestat downregulated the expression of AKR1B10 in NK cells to promote glycolysis and inhibit migration and invasion of HCC cells and metastasis. These findings suggested that Fidarestat is an excellent agent for preventing metastatic spread of HCC in the mouse model. Overall, AKR1B10 could serve as a regulatory target for improving NK cell metabolism in HCC.

MATERIALS AND METHODS

Ethical statement

This experimental procedure and animal use protocol were reviewed and approved by the animal ethics committee of The Second Affiliated Hospital of Kunming Medical University. All animal experiments were performed in accordance with the standard of *The Guide for the Care and Use of Laboratory Animals* published by the National Institutes of Health. Efforts have been made to minimize the suffering of mice.

Nude mouse experiment

Male BALB/c nude mice at 6–8 weeks old (Beijing Institute of Pharmacology, Chinese Academy of Medical Sciences, Beijing, China) were raised in a specific-pathogen-free animal laboratory, with free access to food and water at 22°C–25°C with 60%–80% humidity and a 12 h light/dark cycle. All mice were adaptively fed for one week in the new environment, and their health status was regularly observed. To verify the anti-tumor activity of Fidarestat, 2×10^6 Huh7 cells were inoculated subcutaneously on the right side of nude mice. One week later, 30 nude mice were randomly grouped according to tumor weight (n = 10 each group). Another 30 nude mice were injected with 1×10^6 Huh7 cells via the tail vein and randomly grouped and then randomly intraperitoneally (i.p.) administered with 5 or 10 mg/kg/day Fidarestat or controls for five weeks (n = 10 each group). During the administration period, the tumor volume was measured every five days (tumor volume = 1/2 × length × width^2). Finally, the mice were euthanized, the tumor volumes and weights were measured, and portions of the excised tumor and lung were fixed in 10% neutral formalin for subsequent assays.

In NK cell depletion experiments, 2×10^6 Huh7 cells were inoculated subcutaneously on the right side of nude mice. One week later, 60 nude mice were randomly grouped according to tumor weight (n = 10). To investigate the effect of Fidarestat on tumor metastasis, 60 nude mice were randomly grouped (n = 10), and 1×10^6 Huh7 cells were injected into the nude mice via the tail vein. During the administration, Fidarestat (0.1 mL/10 g) was injected i.p. into mice at a dose of 10 mg/kg, once a day for five weeks, while 150 μg of anti-NK1.1 monoclonal antibody (mAb)-PK136 antibody (HB-191, American Type Culture Collection, VA, USA) or immunoglobulin G (IgG) was administered to the tail vein once a week. Additionally, the tumor volume was measured every five days (tumor volume = 1/2 × length × width^2). Finally, the mice were euthanized, and the tumor volumes and weights were measured. Tissues removed were fixed as described above.

ELISA

An ELISA kit was used to detect IL-2 (PI575, Beyotime Institute of Biotechnology, Shanghai, China), IFN-γ (PI508, Beyotime Institute of Biotechnology), and TNF-α (PT512, Beyotime Institute of Biotechnology) in mouse serum according to the manufacturer's instructions.

Immunohistochemistry (IHC)

The tumor tissues of nude mouse were fixed in formalin; embedded in paraffin; baked at 60°C for 1 h; and then deparaffinized, rehydrated, and immersed in 0.01 M citrate buffer solution. Next, the samples were heated (98°C –100°C) in a microwave, cooled for about 5–10 min, and subjected to two rounds of microwave repair. Next, the samples were blocked with 5% bovine serum albumin (BSA) for 20 min at room temperature, incubated with primary antibody Asialo GM1-NK1.1 (98610001, Wake chemicals, Neuss, Germany) at 37°C for 1 h, and then incubated with secondary antibody (ab6785, Abcam, Cambridge, MA, USA) at 37°C for 15–30 min. After that, the samples were added with streptavidin-biotin complex at 37°C for 30 min, developed with diaminobenzidine at room temperature, and observed under a microscope. Each experiment was repeated three times.

H&E staining

The tissues fixed in 10% neutral formalin were immersed in water overnight, dehydrated, soaked in wax, embedded, and sectioned into slices (5 μm thick). The slices were immersed in water at 40°C for 6 h and then heated at 62°C for 1 h. The slices were immediately immersed in xylene I, xylene II, gradient alcohol, and water for dewaxing and hydration. Next, the slices were stained with hematoxylin for about 8 min, washed with water for counterstain, and stained with eosin for about 2 min. Subsequently, the dyed slices were immersed in gradient alcohol and xylene for dehydration and clearing, sealed with neutral resin, air dried for one day, and finally photographed under a microscope.

Immune cell analysis

After anesthesia with sodium pentobarbital (40 mg/kg, i.p.), the nude mice were euthanized and the tumor tissues were extracted, washed in ice-cold phosphate-buffered saline (PBS), placed in a Petri dish, ground with a syringe tail, and filtered through a 200-mesh screen. The filtrate was then transferred into a 50 mL centrifuge tube for centrifugation at 500 rpm at 4°C for 1 min, and the supernatant was transferred to another 50 mL centrifuge tube for further centrifugation at 4°C followed by removal of the supernatant. Next, the pellet was resuspended in 3 mL of 40% Percoll solution, added into 2 mL of 70% Percoll solution, and centrifuged at 1,260 × *g* at room temperature for 30 min. After centrifugation, the whitish layer was collected, washed twice with PBS, and centrifuged at 4°C to obtain immune cells. The immune cells were separated by immune cell purification kit to obtain MNCs ($CD90^+/CD44^-$), NKT ($CD1d^+/CD3e^+$) cells, NK ($NK1.1^+/CD3^-$) cells, and T ($NK1.1^-/CD3^+$) cells, followed by determination of immune cell proportion through flow cytometry.

NK cell purification and adoptive transfer

For NK cell purification, the NK cells in the transplanted tumor were isolated, counted, resuspended in magnetic-activated cell sorting (MACS) buffer (40 μL/10^7 cells), and blocked with mouse serum for 30 min (4 μL/10^7 cells) to prevent Fc receptor. Next, the NK cells were incubated with biotin-antibody cocktail (Miltenyi Biotec, Bergisch Gladbach, Germany; 10 μL/10^7 cells) in the dark at 4°C for 20 min. The mixture was washed with MACS buffer, centrifuged at 4°C, and resuspended in MACS buffer (70 μL/10^7 cells). Afterward, the NK cells were incubated with Microbeads cocktail (Miltenyi Biotec; 20 μL/10^7 cells) at 4°C for 20 min in the dark, washed with MACS buffer, centrifuged at 4°C, resuspended in MACS buffer, and filtered through Liquid sampling separation columns (Miltenyi Biotec). Subsequently, the eluent was collected and centrifuged to obtain the purified NK cells.

The purified NK cells were cultured in RPMI 1640 medium (Gibco, Carlsbad, CA, USA) containing 10% fetal bovine serum (FBS; Gibco) and 200 U/mL IL-2 (PeproTech, Rocky Hill, NJ, USA) at 37°C and 5% CO_2 for 24 h.

NK cell activation

The purified NK cells were cultured in a medium containing 10% FBS, 200 U/mL IL-2, and 10 ng/mL IL-12 at 37°C and 5% CO_2 for 18 h. During the last 3 h of cytokine action, monensin (10 μg/mL) was added to the medium for further treatment.

NK cell staining

The cells were collected, counted, centrifuged at 4°C, and resuspended in culture medium to adjust the cell density to 2×10^6–2×10^7 cells/mL. Next, 1 mL of cell suspension was transferred to a 24-well plate, incubated with phorbol 12-myristate 13-acetate (PMA; 50 ng/mL, Beyotime Institute of Biotechnology) and ionomycin (1 μg/mL, Beyotime Institute of Biotechnology) at 37°C in 5% CO_2 for 4 h. During the last 3 h of cytokine treatment, monensin (10 μg/mL, Sigma-Aldrich, St. Louis, MO, USA) was added. After that, the cells were collected, centrifuged at 4°C, resuspended in 100 μL of PBS, and blocked with 10 μL of mouse serum for 30 min at 4°C followed by incubation with antibodies at 4°C for 30 min in the dark, including anti-mouse granzyme B (16G6, 12-8822e, eBioscience, San Diego, CA, USA), anti-mouse perforin (eBioOMAK-D, 17-9392, eBioscience), anti-mouse IFN-γ (XMG1.2, 505822, BioLegend, San Diego, CA, USA), and anti-mouse TNF-α (MP6-XT22, 506306, BioLegend). The cells were then fixed with permeabilization buffer at 4°C for 1 h in the dark, washed twice with permeabilization buffer at 4°C, resuspended with 100 μL of permeabilization buffer, and blocked with 10 μL of mouse serum at 4°C for 30 min. NK cells were incubated with antibody at 4°C for 1 h, washed twice with PBS, and resuspended in 200 μL of PBS. The cell suspension was filtered and analyzed by flow cytometry.

Cell culture and infection

HCC cells MHCC97L (MZ-0833; Mingzhou Biotechnology Co., Ltd., Ningbo, Zhejiang, China), Huh7 (MZ-2129; Mingzhou Biotechnology

Co., Ltd.), Hep3B (HB-806; American Type Culture Collection), and Hepa1-6 (CRL-1830; American Type Culture Collection), NK cells (CP-H168; Procell Life Science & Technology Co,. Ltd., Wuhan, Hubei, China), and normal liver cells HL-7702 (Bio-53977; Biobw Biotechnology Co., Ltd., Beijing, China; STR identification as correct) were cultured in Dulbecco's modified Eagle's medium (DMEM) or RPMI 1640 medium (Gibco) containing 10% FBS at 37°C and 5% CO_2. Upon removal of the medium, cells were washed with PBS and trypsinized (Gibco). When cells became round and fell off the walls, a little medium was added to terminate the digestion and the cell suspension was pipetted to wells containing fresh complete medium. In the cytotoxicity experiment, HCC cells and normal liver cells were digested, cultured in a 96-well plate for 24 h, and administered with different concentrations of Fidarestat. Next, the supernatant was tested with the lactate dehydrogenase (LDH) detection kit (Promega, Madison, WI, USA). Cell survival rate (%) = [1 − (release in experimental group − release in blank group)/(release of target cell maximum − release of blank group)] × 100.

For cell infection, when NK cells in the logarithmic growth phase reached 80%–90% confluence, they were trypsinized, resuspended, and seeded into a six-well plate and cultured with 2 mL of complete medium for 24 h. Next, 1 mL of serum-free and antibiotic-free medium was added with overexpressing AKR1B10 lentivirus (MOI 30–40) or negative control (NC) and mixed for cell infection. Subsequently, the cells were cultured for 24 h in the incubator and cultured for 48 h with complete medium for related experiments.

NK cell killing detection *in vitro*

The target cells (Huh7) were counted and prepared as a 2×10^5/mL cell suspension. The suspension was added to a 96-well plate (100 μL/well) and cultured for 24 h. Additionally, activated effector cells (NK cells) were counted, resuspended, and transferred into the 96-well plate according to different MOIs, with 200 μL of total volume per well. Next, the cells were incubated for 4 h at 37°C and 5% CO_2, followed by centrifugation to collect the supernatant for LDH detection. NK cell cytotoxicity (%) = (experimental group release − blank group release)/(target cell maximum release − blank group release) × 100.

ECAR detection

Before detection, the probe plate was incubated with 200 μL of hydration solution at 37°C in a free CO_2 overnight. In addition, 20 μL of polylysine was added into each well at 37°C in a free CO_2 for 2-h incubation. The drug treatment solution was prepared (glucose, 100 mM; Oligomycin A, 10 μM; 2-DG, 500 mM). NK cells were washed with analytical culture, counted, resuspended in analysis medium, and added into the pretreated cell plate (2×10^5 cells/180 μL per well). Then, the cells were centrifuged at 500 × *g* at room temperature for 1 min to promote NK cell attachment in a 37°C, CO_2-free incubator. The probe plate was added with the three drugs (glucose, 20 μL; Oligomycin A, 22 μL; 2-DG, 25 μL), with the remaining wells added with an equal volume of analysis medium. After that, ECAR was determined with Seahorse XFe96 Analyzer (Agilent Technologies, Santa Clara, CA, USA).

Western blot

The cells were collected upon trypsin digestion and lysed with enhanced radio immunoprecipitation assay (RIPA) lysis buffer containing protease inhibitors (Beyotime Institute of Biotechnology). The protein concentration was determined using a bicinchoninic acid protein quantification kit (Beyotime Institute of Biotechnology). The protein was separated by 10% sodium dodecyl sulfate-polyacrylamide gel electrophoresis and electrotransferred to a polyvinylidene fluoride membrane. The membrane was blocked with 5% BSA at room temperature for 1 h; incubated overnight at 4°C with primary antibodies, including anti-AKR1B10 (ab96417, Abcam) and anti-α-Tubulin (ab7291, Abcam); and incubated with horseradish-peroxidase-labeled goat anti-rabbit secondary antibody (Abcam) at room temperature for 1 h. Next, the blots were developed with enhanced chemiluminescence (Millipore, MA, USA) at room temperature for 1 min. Following removing excessive enhanced chemiluminescence, the blots were observed by a visualizer (Tanon 1600, Tanon, Shanghai, China).

Scratch test

Huh7 cells were taken as target cells and NK cells as effector cells. The ratio of target cells to effector cells was set as 1:10. The target cells were counted and added into the culture plate at 1×10^6 cells/well in a medium containing 10% FBS overnight. The differently treated NK cells were incubated in the culture plate at 1×10^6 cells/well for 4 h, centrifuged to separate the NK cells in the supernatant, and cultured for another 20 h. The scratches were measured under an optical microscope and photographed under an inverted microscope.

Transwell assay

The Huh7 cells were cultured in a serum-free medium for 12 h and then resuspended in serum-free medium (1×10^5 cells/mL). Next, 100 μL of Huh7 cell suspension was transferred to apical chamber of Transwell chamber coated with Matrigel (Becton Dickinson, NJ, USA), and NK cells were added to the basolateral chamber (1×10^4 cells/well) at 37°C for 4 h. Next, the suspended NK cells in the basolateral chamber were discarded, and Huh7 cells were cultured for 20 h. The cells not invading the Matrigel membrane were fixed with 100% methanol, stained with 1% toluidine blue (Sigma-Aldrich), and counted under an inverted light microscope (Carl Zeiss, Thornwood, NY, USA) within five randomly selected fields. Each experiment was repeated three times.

Statistical analysis

The experimental data were presented as mean ± standard deviation and analyzed by un-paired t test, one-way or two-way or repeated-measures analysis of variance (ANOVA), and Turkey's post hoc test through Prism 8.0.1 software (GraphPad, San Diego, CA, USA). A *$p < 0.05$ means significant difference.

SUPPLEMENTAL INFORMATION

Supplemental information can be found online at https://doi.org/10.1016/j.omto.2021.06.005.

ACKNOWLEDGMENTS

We appreciate the reviewers for critical comments on this article. This work was supported by the grants from the National Natural Science Foundation of China (81660399 and 81860423); the Medical Leading Talent Project of Yunnan Province (L201622); and Yunnan Provincial Clinical Center of Hepato-Biliary-Pancreatic Diseases (no specific number) to L.W.; the Applied Fundamental Research Joint Program of Science & Technology Department of Yunnan Province and Kunming Medical University (Youth PhD Fund; 202001AY0700001-147); the Leading Academic and Technical Young and Mid-Aged Program of Kunming Medical University (60118260108) to Y.K.; Scientific Research Foundation of the Department of Education of Yunnan Province (2019J1253) to H.T.; and PhD Student Innovation Fund of Kunming Medical University (2020D007) to T.W.

AUTHOR CONTRIBUTIONS

T.W., Y.K., H.T., and C.L. designed the study. L.W. collated the data, designed and developed the database, carried out data analyses, and produced the initial draft of the manuscript. T.W., J.L., and Y.K. contributed to drafting the manuscript. All authors have read and approved the final submitted manuscript.

DECLARATION OF INTERESTS

The authors declare no competing interests.

REFERENCES

1. Balogh, J., Victor, D., 3rd, Asham, E.H., Burroughs, S.G., Boktour, M., Saharia, A., Li, X., Ghobrial, R.M., and Monsour, H.P., Jr. (2016). Hepatocellular carcinoma: a review. J. Hepatocell. Carcinoma *3*, 41–53.
2. Petrick, J.L., Kelly, S.P., Altekruse, S.F., McGlynn, K.A., and Rosenberg, P.S. (2016). Future of Hepatocellular Carcinoma Incidence in the United States Forecast Through 2030. J. Clin. Oncol. *34*, 1787–1794.
3. Omata, M., Cheng, A.L., Kokudo, N., Kudo, M., Lee, J.M., Jia, J., Tateishi, R., Han, K.H., Chawla, Y.K., Shiina, S., et al. (2017). Asia-Pacific clinical practice guidelines on the management of hepatocellular carcinoma: a 2017 update. Hepatol. Int. *11*, 317–370.
4. Friemel, J., Rechsteiner, M., Frick, L., Böhm, F., Struckmann, K., Egger, M., Moch, H., Heikenwalder, M., and Weber, A. (2015). Intratumor heterogeneity in hepatocellular carcinoma. Clin. Cancer Res. *21*, 1951–1961.
5. Cicinnati, V.R., Sotiropoulos, G.C., and Beckebaum, S. (2010). Established and emerging therapies for hepatocellular carcinoma. Minerva Med. *101*, 405–418.
6. Zhang, B., and Finn, R.S. (2016). Personalized Clinical Trials in Hepatocellular Carcinoma Based on Biomarker Selection. Liver Cancer *5*, 221–232.
7. Biswas, S.K. (2015). Metabolic Reprogramming of Immune Cells in Cancer Progression. Immunity *43*, 435–449.
8. Leone, R.D., and Powell, J.D. (2020). Metabolism of immune cells in cancer. Nat. Rev. Cancer *20*, 516–531.
9. Sun, C., Sun, H.Y., Xiao, W.H., Zhang, C., and Tian, Z.G. (2015). Natural killer cell dysfunction in hepatocellular carcinoma and NK cell-based immunotherapy. Acta Pharmacol. Sin. *36*, 1191–1199.
10. Cai, L., Zhang, Z., Zhou, L., Wang, H., Fu, J., Zhang, S., Shi, M., Zhang, H., Yang, Y., Wu, H., et al. (2008). Functional impairment in circulating and intrahepatic NK cells and relative mechanism in hepatocellular carcinoma patients. Clin. Immunol. *129*, 428–437.
11. Terrén, I., Orrantia, A., Vitallé, J., Zenarruzabeitia, O., and Borrego, F. (2019). NK Cell Metabolism and Tumor Microenvironment. Front. Immunol. *10*, 2278.
12. Heringlake, S., Hofdmann, M., Fiebeler, A., Manns, M.P., Schmiegel, W., and Tannapfel, A. (2010). Identification and expression analysis of the aldo-ketoreductase1-B10 gene in primary malignant liver tumours. J. Hepatol. *52*, 220–227.
13. Chung, Y.T., Matkowskyj, K.A., Li, H., Bai, H., Zhang, W., Tsao, M.S., Liao, J., and Yang, G.Y. (2012). Overexpression and oncogenic function of aldo-keto reductase family 1B10 (AKR1B10) in pancreatic carcinoma. Mod. Pathol. *25*, 758–766.
14. Ma, J., Luo, D.X., Huang, C., Shen, Y., Bu, Y., Markwell, S., Gao, J., Liu, J., Zu, X., Cao, Z., et al. (2012). AKR1B10 overexpression in breast cancer: association with tumor size, lymph node metastasis and patient survival and its potential as a novel serum marker. Int. J. Cancer *131*, E862–E871.
15. Sonohara, F., Inokawa, Y., Hishida, M., Kanda, M., Nishikawa, Y., Yamada, S., Fujii, T., Sugimoto, H., Kodera, Y., and Nomoto, S. (2016). Prognostic significance of AKR1B10 gene expression in hepatocellular carcinoma and surrounding nontumorous liver tissue. Oncol. Lett. *12*, 4821–4828.
16. Yao, H.B., Xu, Y., Chen, L.G., Guan, T.P., Ma, Y.Y., He, X.J., Xia, Y.J., Tao, H.Q., and Shao, Q.S. (2014). AKR1B10, a good prognostic indicator in gastric cancer. Eur. J. Surg. Oncol. *40*, 318–324.
17. Ha, S.Y., Song, D.H., Lee, J.J., Lee, H.W., Cho, S.Y., and Park, C.K. (2014). High expression of aldo-keto reductase 1B10 is an independent predictor of favorable prognosis in patients with hepatocellular carcinoma. Gut Liver *8*, 648–654.
18. Shi, J., Chen, L., Chen, Y., Lu, Y., Chen, X., and Yang, Z. (2019). Aldo-Keto Reductase Family 1 Member B10 (AKR1B10) overexpression in tumors predicts worse overall survival in hepatocellular carcinoma. J. Cancer *10*, 4892–4901.
19. Wang, J., Zhou, Y., Fei, X., Chen, X., and Chen, Y. (2018). Biostatistics mining associated method identifies AKR1B10 enhancing hepatocellular carcinoma cell growth and degenerated by miR-383-5p. Sci. Rep. *8*, 11094.
20. Ohashi, T., Idogawa, M., Sasaki, Y., Suzuki, H., and Tokino, T. (2013). AKR1B10, a transcriptional target of p53, is downregulated in colorectal cancers associated with poor prognosis. Mol. Cancer Res. *11*, 1554–1563.
21. Ruiz, F.X., Cousido-Siah, A., Mitschler, A., Farrés, J., Parés, X., and Podjarny, A. (2013). X-ray structure of the V301L aldo-keto reductase 1B10 complexed with NADP(+) and the potent aldose reductase inhibitor fidarestat: implications for inhibitor binding and selectivity. Chem. Biol. Interact. *202*, 178–185.
22. Ramunno, A., Cosconati, S., Sartini, S., Maglio, V., Angiuoli, S., La Pietra, V., Di Maro, S., Giustiniano, M., La Motta, C., Da Settimo, F., et al. (2012). Progresses in the pursuit of aldose reductase inhibitors: the structure-based lead optimization step. Eur. J. Med. Chem. *51*, 216–226.
23. Tammali, R., Reddy, A.B., Saxena, A., Rychahou, P.G., Evers, B.M., Qiu, S., Awasthi, S., Ramana, K.V., and Srivastava, S.K. (2011). Inhibition of aldose reductase prevents colon cancer metastasis. Carcinogenesis *32*, 1259–1267.
24. Barrow, A.D., Edeling, M.A., Trifonov, V., Luo, J., Goyal, P., Bohl, B., Bando, J.K., Kim, A.H., Walker, J., Andahazy, M., et al. (2018). Natural Killer Cells Control Tumor Growth by Sensing a Growth Factor. Cell *172*, 534–548.e19.
25. Cong, J., Wang, X., Zheng, X., Wang, D., Fu, B., Sun, R., Tian, Z., and Wei, H. (2018). Dysfunction of Natural Killer Cells by FBP1-Induced Inhibition of Glycolysis during Lung Cancer Progression. Cell Metab. *28*, 243–255.e5.
26. van Weverwijk, A., Koundouros, N., Iravani, M., Ashenden, M., Gao, Q., Poulogiannis, G., Jungwirth, U., and Isacke, C.M. (2019). Metabolic adaptability in metastatic breast cancer by AKR1B10-dependent balancing of glycolysis and fatty acid oxidation. Nat. Commun. *10*, 2698.
27. Satriano, L., Lewinska, M., Rodrigues, P.M., Banales, J.M., and Andersen, J.B. (2019). Metabolic rearrangements in primary liver cancers: cause and consequences. Nat. Rev. Gastroenterol. Hepatol. *16*, 748–766.
28. Kubes, P., and Jenne, C. (2018). Immune Responses in the Liver. Annu. Rev. Immunol. *36*, 247–277.
29. DiStefano, J.K., and Davis, B. (2019). Diagnostic and Prognostic Potential of AKR1B10 in Human Hepatocellular Carcinoma. Cancers (Basel) *11*, 486.
30. Tammali, R., Srivastava, S.K., and Ramana, K.V. (2011). Targeting aldose reductase for the treatment of cancer. Curr. Cancer Drug Targets *11*, 560–571.
31. Yadav, U.C., Aguilera-Aguirre, L., Ramana, K.V., Boldogh, I., and Srivastava, S.K. (2010). Aldose reductase inhibition prevents metaplasia of airway epithelial cells. PLoS ONE *5*, e14440.

32. Sun, H., Sun, C., Tian, Z., and Xiao, W. (2013). NK cells in immunotolerant organs. Cell. Mol. Immunol. *10*, 202–212.

33. Nayyar, G., Chu, Y., and Cairo, M.S. (2019). Overcoming Resistance to Natural Killer Cell Based Immunotherapies for Solid Tumors. Front. Oncol. *9*, 51.

34. Wu, Y., Kuang, D.M., Pan, W.D., Wan, Y.L., Lao, X.M., Wang, D., Li, X.F., and Zheng, L. (2013). Monocyte/macrophage-elicited natural killer cell dysfunction in hepatocellular carcinoma is mediated by CD48/2B4 interactions. Hepatology *57*, 1107–1116.

35. Yang, J., Pemberton, A., Morrison, W.I., and Connelley, T. (2018). Granzyme B Is an Essential Mediator in CD8(+) T Cell Killing of Theileria parva-Infected Cells. Infect. Immun. *87*, e00386-18.

36. Qian, X., Shi, Z., Qi, H., Zhao, M., Huang, K., Han, D., Zhou, J., Liu, C., Liu, Y., Lu, Y., et al. (2019). A novel Granzyme B nanoparticle delivery system simulates immune cell functions for suppression of solid tumors. Theranostics *9*, 7616–7627.

37. Gerada, C., Steain, M., Campbell, T.M., McSharry, B., Slobedman, B., and Abendroth, A. (2019). Granzyme B Cleaves Multiple Herpes Simplex Virus 1 and Varicella-Zoster Virus (VZV) Gene Products, and VZV ORF4 Inhibits Natural Killer Cell Cytotoxicity. J. Virol. *93*, e01140-19.

38. Shibata, Y., Hara, T., Nagano, J., Nakamura, N., Ohno, T., Ninomiya, S., Ito, H., Tanaka, T., Saito, K., Seishima, M., et al. (2016). The Role of Indoleamine 2,3-Dioxygenase in Diethylnitrosamine-Induced Liver Carcinogenesis. PLoS ONE *11*, e0146279.

39. Kapoor, S. (2013). AKR1B10 and its emerging role in tumor carcinogenesis and as a cancer biomarker. Int. J. Cancer *132*, 495.

40. Wang, C., Yan, R., Luo, D., Watabe, K., Liao, D.F., and Cao, D. (2009). Aldo-keto reductase family 1 member B10 promotes cell survival by regulating lipid synthesis and eliminating carbonyls. J. Biol. Chem. *284*, 26742–26748.

41. Takemura, M., Endo, S., Matsunaga, T., Soda, M., Zhao, H.T., El-Kabbani, O., Tajima, K., Iinuma, M., and Hara, A. (2011). Selective inhibition of the tumor marker aldo-keto reductase family member 1B10 by oleanolic acid. J. Nat. Prod. *74*, 1201–1206.

42. Soda, M., Hu, D., Endo, S., Takemura, M., Li, J., Wada, R., Ifuku, S., Zhao, H.T., El-Kabbani, O., Ohta, S., et al. (2012). Design, synthesis and evaluation of caffeic acid phenethyl ester-based inhibitors targeting a selectivity pocket in the active site of human aldo-keto reductase 1B10. Eur. J. Med. Chem. *48*, 321–329.

43. Petrova, V., Annicchiarico-Petruzzelli, M., Melino, G., and Amelio, I. (2018). The hypoxic tumour microenvironment. Oncogenesis *7*, 10.

44. Hasmim, M., Messai, Y., Ziani, L., Thiery, J., Bouhris, J.H., Noman, M.Z., and Chouaib, S. (2015). Critical Role of Tumor Microenvironment in Shaping NK Cell Functions: Implication of Hypoxic Stress. Front. Immunol. *6*, 482.

45. Parodi, M., Raggi, F., Cangelosi, D., Manzini, C., Balsamo, M., Blengio, F., Eva, A., Varesio, L., Pietra, G., Moretta, L., et al. (2018). Hypoxia Modifies the Transcriptome of Human NK Cells, Modulates Their Immunoregulatory Profile, and Influences NK Cell Subset Migration. Front. Immunol. *9*, 2358.

46. Morse, M.A., Sun, W., Kim, R., He, A.R., Abada, P.B., Mynderse, M., and Finn, R.S. (2019). The Role of Angiogenesis in Hepatocellular Carcinoma. Clin. Cancer Res. *25*, 912–920.

47. Tammali, R., Reddy, A.B., Srivastava, S.K., and Ramana, K.V. (2011). Inhibition of aldose reductase prevents angiogenesis in vitro and in vivo. Angiogenesis *14*, 209–221.